


## Stability of $(N + 1)$ -body fermion clusters in a multiband Hubbard model

M. Iskin<sup>1</sup> and A. Keleş<sup>2</sup> 

<sup>1</sup>*Department of Physics, Koç University, Rumelifeneri Yolu, 34450 Sarıyer, Istanbul, Turkey*

<sup>2</sup>*Department of Physics, Middle East Technical University, Ankara 06800, Turkey*



(Received 19 April 2022; accepted 22 August 2022; published 6 September 2022)

We start with a variational approach and derive a set of coupled integral equations for the bound states of  $N$  identical spin- $\uparrow$  fermions and a single spin- $\downarrow$  fermion in a generic multiband Hubbard Hamiltonian with an attractive on-site interaction. As an illustration, we apply our integral equations to the one-dimensional sawtooth lattice up to  $N \leq 3$ , i.e., to the  $(3 + 1)$ -body problem, and we reveal not only the presence of tetramer states in this two-band model but also their quasiflat dispersion when formed in a flat band. Furthermore, for  $N = \{4, 5, \dots, 10\}$ , our density-matrix renormalization-group simulations and exact diagonalization suggest the presence of larger and larger multimers with lower and lower binding energies, conceivably without an upper bound on  $N$ . These peculiar  $(N + 1)$ -body clusters are in sharp contrast with the exact results on the single-band linear-chain model where none of the  $N \geq 2$  multimers appear. Hence their presence must be taken into account for a proper description of the many-body phenomena in flat-band systems, e.g., they may suppress superconductivity especially when there exists a large spin imbalance.

DOI: [10.1103/PhysRevA.106.033304](https://doi.org/10.1103/PhysRevA.106.033304)

### I. INTRODUCTION

Exactly solvable few-body problems offer a unique avenue to gain valuable insights into the microscopic origins of novel many-body phenomena, starting from a collection of isolated composites such as dimers, trimers, and other multimers [1–7]. The archetypal example is the instability of a noninteracting Fermi gas against the formation of Cooper pairs, which eventually leads the way to the theory of BCS superconductivity. It turns out a dimer that is formed between a spin-up and a spin-down fermion (assuming they have equal masses) is the only stable bound state in the presence of an attractive contact interaction, suggesting that the underlying Cooper-pairing mechanism is robust for the BCS theory in all dimensions [7]. In sharp contrast with this conventional insight, here we show that the multimers may also play a decisive role in a multiband system, especially when there exists a flat band in the spectrum.

Until recently, all of the few-body studies were focused either on continuum systems or on their lattice counterparts that feature only a single band. As an example, three identical bosonic atoms that are interacting via short-range resonant interactions in vacuum are known to exhibit an infinite series of three-body bound states, i.e., the so-called Efimov effect [1–7]. The experimental realization of this long-sought trimer state with ultracold bosons [8–12] has sparked a growing interest in related effects with fermions. For instance, three-body, four-body, and five-body Efimov effects have all been predicted, respectively, with two, three and four identical heavy fermions that are interacting resonantly with a much lighter particle [13–20]. Thus, unlike the equal-mass case in which only dimer states are allowed, the multimer (trimer, tetramer, and pentamer) states appear in mass-imbalanced

mixtures when the mass ratio exceeds a certain threshold depending on the multimer type. See recent reviews for a comprehensive list of related works from atomic, molecular, and optical physics to condensed-matter, nuclear, and particle physics [1–6]. Analogous predictions were also reported for the appearance of trimer states in single-band lattices but only when the tunneling amplitudes are spin-dependent [21–25].

Despite all of this progress, it is surprising that few-body physics is still in its infancy in a more realistic lattice model when there exists more than one Bloch band in the one-body spectrum. For instance, as opposed to the exact results on the single-band linear chain, which allow only dimers [7,21,22,26], the energetic stability of the trimers has recently been predicted in a sawtooth lattice that features two bands [27,28]. Remarkably, these trimers have a quasiflat dispersion with a negligible bandwidth when they form in a flat band, which is very different from the highly dispersive spectrum of the underlying dimers. In this paper, we study the bound states of  $N$  identical spin- $\uparrow$  fermions and a single spin- $\downarrow$  fermion in a generic multiband Hubbard model with an attractive on-site interaction. We start with a variational approach, and we derive a set of exact results that are readily applicable to all lattice geometries in all dimensions. As an illustration, we apply our  $N \leq 3$  theory to the sawtooth lattice, and we reveal both the energetic stability of the tetramer states and their quasiflat dispersion when formed in a flat band. Furthermore, we perform density-matrix renormalization-group (DMRG) simulations and exact diagonalization to investigate the possibility of larger bound states, and we present strong evidence for the energetic stability of the multimer states with  $N = \{4, 5, \dots, 10\}$ , conceivably without an upper bound on  $N$ .

Given the recent surge of experimental and theoretical interest in flat-band systems [29–41], which is boosted by the discovery of superconductivity and correlated insulating states in the magic-angle twisted bilayer graphene (MATBG) systems [42], we hope that our peculiar findings will trigger further interest in the few-body aspects of kagomé and Lieb-like toy models that exhibit a flat band in their spectrum [43]. Furthermore, one of the profound implications of our findings is that the Cooper-pairing based theories of superconductivity in flat-band systems may not always be the best starting point, i.e., the formation of multimers may suppress superconductivity in these systems, especially when there exists a large spin imbalance. Thus our exact few-body results will shed some light on the proper description of the many-body phenomena in flat-band systems.

The rest of this paper is organized as follows. In Sec. II we first introduce the multiband Hubbard model and then derive the integral equations for the  $(N + 1)$ -body problem through a variational approach. In Sec. III we apply our variational results to the sawtooth lattice, and we discuss the full  $(1 + 1)$ -body spectrum, the full  $(2 + 1)$ -body spectrum, and the ground state of tetramers. There we also analyze ground states of pentamers and other multimers with DMRG simulations and exact diagonalization. In Sec. IV we end the paper with a brief summary of our results and outlook. As for the Appendixes, the numerical implementation of the  $(3 + 1)$ -body problem is described in Appendix A, the low-energy excitation energies from the exact diagonalization are presented in Appendix B, and the fermion-boson mapping in the three-body problem is illustrated in Appendix C.

## II. $(N + 1)$ -BODY PROBLEM

In this paper, we are interested in the role of multiple Bloch bands in the energetic stability of the multimer states. For this purpose, we consider few-body bound states that are made of  $N$  spin- $\uparrow$  fermions and a single spin- $\downarrow$  fermion in a multiband Hubbard model.

### A. Multiband Hubbard model

The standard Hubbard Hamiltonian [37,44]  $\mathcal{H} = \sum_{\sigma} \mathcal{H}_{\sigma} + \mathcal{H}_{\uparrow\downarrow}$  is made of two terms:

$$\mathcal{H}_{\sigma} = - \sum_{Si,S'i'} t_{Si,S'i'}^{\sigma} c_{Si\sigma}^{\dagger} c_{S'i'\sigma}, \quad (1)$$

$$\mathcal{H}_{\uparrow\downarrow} = -U \sum_{Si} c_{Si\uparrow}^{\dagger} c_{Si\downarrow}^{\dagger} c_{Si\downarrow} c_{Si\uparrow}. \quad (2)$$

Here the first term accounts for the kinetic energy of the spin- $\sigma$  fermions where the hopping parameter  $t_{Si,S'i'}^{\sigma}$  describes their tunneling amplitude from the sublattice (or basis or orbital) site  $S'$  in the unit cell  $i'$  to the sublattice site  $S$  in the unit cell  $i$ . On the other hand, the second term accounts for the potential energy of the system, where  $U \geq 0$  is the strength of the attractive interaction between  $\uparrow$  and  $\downarrow$  fermions when they are on the same site. Next we use a canonical transformation, i.e.,

$$c_{Si\sigma}^{\dagger} = \frac{1}{\sqrt{N_c}} \sum_{\mathbf{k}} e^{-i\mathbf{k} \cdot \mathbf{r}_{Si}} c_{S\mathbf{k}\sigma}^{\dagger}, \quad (3)$$

and we express the Hubbard Hamiltonian in the reciprocal lattice, where  $N_c$  is the number of unit cells in the system,  $\mathbf{k}$  is the crystal momentum in the first Brillouin zone (BZ), and  $\mathbf{r}_{Si}$  is the position of the sublattice site  $S$  in unit cell  $i$ . Note that the total number of lattice sites is  $N_s = N_b N_c$  when the number of sublattice sites in a unit cell is  $N_b$ . In addition, noting that  $c_{n\mathbf{k}\sigma}^{\dagger} = \sum_S n_{S\mathbf{k}\sigma} c_{S\mathbf{k}\sigma}^{\dagger}$ , where  $n$  is the band index for the Bloch bands (there are  $N_b$  of them) and  $n_{S\mathbf{k}\sigma}$  is the projection of the Bloch state onto the sublattice  $S$ , we eventually find [45]

$$\mathcal{H}_{\sigma} = \sum_{n\mathbf{k}} \varepsilon_{n\mathbf{k}\sigma} c_{n\mathbf{k}\sigma}^{\dagger} c_{n\mathbf{k}\sigma}, \quad (4)$$

$$\mathcal{H}_{\uparrow\downarrow} = \frac{1}{N_c} \sum_{\substack{nm'm' \\ \mathbf{k}\mathbf{k}'\mathbf{q}}} V_{n'm'\mathbf{k}'}^{nm\mathbf{k}}(\mathbf{q}) b_{nm}^{\dagger}(\mathbf{k}, \mathbf{q}) b_{n'm'}(\mathbf{k}', \mathbf{q}). \quad (5)$$

Here  $\varepsilon_{n\mathbf{k}\sigma}$  is the one-body dispersion of the fermions in band  $n$ ,  $V_{n'm'\mathbf{k}'}^{nm\mathbf{k}}(\mathbf{q}) = -U \sum_S n_{S,\mathbf{k}+\frac{\mathbf{q}}{2},\uparrow}^* m_{S,-\mathbf{k}+\frac{\mathbf{q}}{2},\downarrow}^* m'_{S,-\mathbf{k}'+\frac{\mathbf{q}}{2},\downarrow} n'_{S,\mathbf{k}'+\frac{\mathbf{q}}{2},\uparrow}$  characterizes the on-site interactions in momentum space, and  $b_{nm}^{\dagger}(\mathbf{k}, \mathbf{q}) = c_{n,\mathbf{k}+\frac{\mathbf{q}}{2},\uparrow}^{\dagger} c_{m,-\mathbf{k}+\frac{\mathbf{q}}{2},\downarrow}^{\dagger}$  creates a pair of fermions in the Bloch bands.

### B. Variational approach

Motivated by the success of the variational approach on the two-body and three-body problems [28,45,46], here we attack the  $(N + 1)$ -body problem with the following ansatz:

$$\mathcal{H}|\Psi_{\mathbf{q}}\rangle = E_{N+1}^{\mathbf{q}}|\Psi_{\mathbf{q}}\rangle, \quad (6)$$

$$|\Psi_{\mathbf{q}}\rangle = \sum_{\substack{n_1 \dots n_N m \\ \mathbf{k}_1 \dots \mathbf{k}_N}} \alpha_{n_1 \dots n_N m}^{\mathbf{k}_1 \dots \mathbf{k}_N}(\mathbf{q}) \left( \prod_{i=1}^N c_{n_i \mathbf{k}_i \uparrow}^{\dagger} \right) c_{m \mathbf{Q} \downarrow}^{\dagger} |0\rangle. \quad (7)$$

Here the ansatz  $|\Psi_{\mathbf{q}}\rangle$  explicitly conserves the center-of-mass (COM) momentum  $\mathbf{q}$  of the particles,  $E_{N+1}^{\mathbf{q}}$  is the energy of the  $(N + 1)$ -body bound state,  $\alpha_{n_1 \dots n_N m}^{\mathbf{k}_1 \dots \mathbf{k}_N}(\mathbf{q})$  is the variational complex parameter, and

$$\mathbf{Q} = \mathbf{q} - \sum_{i=1}^N \mathbf{k}_i \quad (8)$$

is defined for convenience. Since  $|\Psi_{\mathbf{q}}\rangle$  has the most general form, it will provide us with the exact solution. The normalization condition can be written as  $\langle \Psi_{\mathbf{q}} | \Psi_{\mathbf{q}} \rangle = N! \sum_{\substack{n_1 \dots n_N m \\ \mathbf{k}_1 \dots \mathbf{k}_N}} |\alpha_{n_1 \dots n_N m}^{\mathbf{k}_1 \dots \mathbf{k}_N}(\mathbf{q})|^2$ , where we enforce the Pauli principle, and we make extensive use of

$$\alpha_{n_1 \dots n_i \dots n_j \dots n_N m}^{\mathbf{k}_1 \dots \mathbf{k}_i \dots \mathbf{k}_j \dots \mathbf{k}_N}(\mathbf{q}) = -\alpha_{n_1 \dots n_j \dots n_i \dots n_N m}^{\mathbf{k}_1 \dots \mathbf{k}_j \dots \mathbf{k}_i \dots \mathbf{k}_N}(\mathbf{q}), \quad (9)$$

i.e., the ansatz picks up a minus sign under the exchange of a pair of its spin- $\uparrow$  fermions. After a lengthy but straightforward calculation, we find

$$\langle \mathcal{H}_{\uparrow} \rangle = N! \sum_{\substack{n_1 \dots n_N m \\ \mathbf{k}_1 \dots \mathbf{k}_N}} |\alpha_{n_1 \dots n_N m}^{\mathbf{k}_1 \dots \mathbf{k}_N}(\mathbf{q})|^2 \left( \sum_{i=1}^N \varepsilon_{n_i \mathbf{k}_i \uparrow} \right), \quad (10)$$

$$\langle \mathcal{H}_{\downarrow} \rangle = N! \sum_{\substack{n_1 \dots n_N m \\ \mathbf{k}_1 \dots \mathbf{k}_N}} |\alpha_{n_1 \dots n_N m}^{\mathbf{k}_1 \dots \mathbf{k}_N}(\mathbf{q})|^2 \varepsilon_{m \mathbf{Q} \downarrow}, \quad (11)$$

$$\begin{aligned} \langle \mathcal{H}_{\uparrow\downarrow} \rangle &= -\frac{N!U}{N_c} \sum_{\substack{n_1 \dots n_N m_1 m_2 \\ S \mathbf{k}_1 \dots \mathbf{k}_N \mathbf{k}}} \alpha_{n_1 \dots n_N m_1}^{\mathbf{k}_1 \dots \mathbf{k}_N}(\mathbf{q}) n_{S \mathbf{k}_1 \uparrow}^* m_{1 S \mathbf{Q} \downarrow} \\ &\times \sum_{i=1}^N \left\{ \sum_{n_i \mathbf{k}_i} [\alpha_{n_1 \dots n_N m_2}^{\mathbf{k}_1 \dots \mathbf{k}_N}(\mathbf{q})]^* m_{2 S \mathbf{Q} \downarrow}^* \delta_{n_i n} \delta_{\mathbf{k}_i \mathbf{k}} \right\} n_{i S \mathbf{k}_i \uparrow} \end{aligned} \quad (12)$$

for the expectation value of the multiband Hubbard Hamiltonian. Here  $*$  is for the complex conjugation and  $\delta_{ij}$  is the Kronecker delta.

$$\gamma_{n_2 \dots n_N S}^{\mathbf{k}_2 \dots \mathbf{k}_N}(\mathbf{q}) = \frac{U}{N_c} \sum_{n_1 m S' \mathbf{k}_1} \frac{m_{S' \mathbf{Q} \downarrow}^* m_{S \mathbf{Q} \downarrow} n_{1 S \mathbf{k}_1 \uparrow}}{(\sum_{i=1}^N \varepsilon_{n_i \mathbf{k}_i \uparrow}) + \varepsilon_{m \mathbf{Q} \downarrow} - E_{N+1}^{\mathbf{q}}} \left\{ n_{1 S' \mathbf{k}_1 \uparrow}^* \gamma_{n_2 \dots n_N S'}^{\mathbf{k}_2 \dots \mathbf{k}_N}(\mathbf{q}) - \sum_{i=2}^N n_{i S' \mathbf{k}_i \uparrow}^* \left[ \sum_{n_i \mathbf{k}_i} \gamma_{n_2 \dots n_N S'}^{\mathbf{k}_2 \dots \mathbf{k}_N}(\mathbf{q}) \delta_{n_i n_1} \delta_{\mathbf{k}_i \mathbf{k}_1} \right] \right\}. \quad (14)$$

This exact expression is one of our central results in this work: the  $(N + 1)$ -body problem in a multiband Hubbard model is reduced to the solutions of  $N_b^N$  coupled integral equations with  $N - 1$  momentum variables for a given set of parameters, i.e.,  $\mathbf{q}$ ,  $U$ , and hoppings. Its continuum version is recovered by setting the Bloch factors to unity and dropping the band as well as sublattice indices, i.e., it requires the solution of a single integral equation for  $\gamma^{\mathbf{k}_2 \dots \mathbf{k}_N}(\mathbf{q})$ ; Ref. [20] [Eq. (3)] and Ref. [47] for details. Once  $E_{N+1}^{\mathbf{q}}$  is obtained, the binding energy of the  $(N + 1)$ -body bound state can be determined by

$$E_{N+1}^{\text{be}}(\mathbf{q}) = -E_{N+1}^{\mathbf{q}} + \min \{ E_{(N-1)+1}^{\mathbf{q}'} + \varepsilon_{n, \mathbf{q}-\mathbf{q}'} \uparrow \}. \quad (15)$$

This is because while an  $(N + 1)$ -body bound state may in general become energetically unstable against dissociation into an  $[(N - \ell) + 1]$ -body bound state and  $\ell$  free spin- $\uparrow$  fermions, the  $\ell = 1$  process is closest in energy to  $E_{N+1}^{\mathbf{q}}$  when the  $[(N - 1) + 1]$ -body bound state is energetically stable, i.e.,  $E_N^{\text{be}}(\mathbf{q}) > 0$ , to begin with [48]. Indeed, this turns out to be the case for all of the multimers in the flat band of the sawtooth lattice discussed below.

Let us first show that Eq. (14) reproduces the available literature in the  $N = 1$  and 2 cases. For  $N = 1$ , since the summation term of the second line is irrelevant, Eq. (14) is equivalent to

$$\gamma_S(\mathbf{q}) = \frac{U}{N_c} \sum_{n_1 m S' \mathbf{k}_1} \frac{m_{S' \mathbf{Q} \downarrow}^* m_{S \mathbf{Q} \downarrow} n_{1 S \mathbf{k}_1 \uparrow} n_{1 S' \mathbf{k}_1 \uparrow}^*}{\varepsilon_{n_1 \mathbf{k}_1 \uparrow} + \varepsilon_{m \mathbf{Q} \downarrow} - E_2^{\mathbf{q}}} \gamma_{S'}(\mathbf{q}), \quad (16)$$

where  $\mathbf{Q} = \mathbf{q} - \mathbf{k}_1$ . This self-consistency relation can be recast as an eigenvalue problem of an  $N_b \times N_b$  matrix, giving rise to  $N_b$  branches for the two-body dispersion  $E_2^{\mathbf{q}}$  for each given  $\mathbf{q}$ . See Ref. [27] for an alternative derivation with a different approach. Equation (16) is recently used to reveal a deeper connection between the effective-mass tensor of the lowest-lying dimer states and the quantum-metric tensor of the underlying Bloch states [45,46,49]. For  $N = 2$ , Eq. (14) reduces to

$$\begin{aligned} \gamma_{n_2 S}^{\mathbf{k}_2}(\mathbf{q}) &= \frac{U}{N_c} \sum_{n_1 m S' \mathbf{k}_1} \frac{m_{S' \mathbf{Q} \downarrow}^* m_{S \mathbf{Q} \downarrow} n_{1 S \mathbf{k}_1 \uparrow}}{\varepsilon_{n_1 \mathbf{k}_1 \uparrow} + \varepsilon_{n_2 \mathbf{k}_2 \uparrow} + \varepsilon_{m \mathbf{Q} \downarrow} - E_3^{\mathbf{q}}} \\ &\times [n_{1 S' \mathbf{k}_1 \uparrow}^* \gamma_{n_2 S'}^{\mathbf{k}_2}(\mathbf{q}) - n_{2 S' \mathbf{k}_2 \uparrow}^* \gamma_{n_1 S'}^{\mathbf{k}_1}(\mathbf{q})], \end{aligned} \quad (17)$$

The variational parameters are determined through the functional minimization of  $\langle \Psi_{\mathbf{q}} | \mathcal{H} - E_{N+1}^{\mathbf{q}} | \Psi_{\mathbf{q}} \rangle$ , but this procedure leads to a complicated expression. To simplify the resultant equations, we define a new parameter set

$$\gamma_{n_2 \dots n_N S}^{\mathbf{k}_2 \dots \mathbf{k}_N}(\mathbf{q}) = \sum_{n_1 m \mathbf{k}_1} \alpha_{n_1 \dots n_N m}^{\mathbf{k}_1 \dots \mathbf{k}_N}(\mathbf{q}) n_{1 S \mathbf{k}_1 \uparrow} m_{S \mathbf{Q} \downarrow}, \quad (13)$$

and we make use of Pauli exchange statistics  $\gamma_{n_2 \dots n_i \dots n_j \dots n_N S}^{\mathbf{k}_2 \dots \mathbf{k}_i \dots \mathbf{k}_j \dots \mathbf{k}_N}(\mathbf{q}) = -\gamma_{n_2 \dots n_j \dots n_i \dots n_N S}^{\mathbf{k}_2 \dots \mathbf{k}_j \dots \mathbf{k}_i \dots \mathbf{k}_N}(\mathbf{q})$ . We finally obtain a set of coupled integral equations with the following structure:

where  $\mathbf{Q} = \mathbf{q} - \mathbf{k}_1 - \mathbf{k}_2$ . This is a set of  $N_b^2$  coupled integral equations with one momentum variable, and it can be recast as an eigenvalue problem of an  $N_b^2 N_c \times N_b^2 N_c$  matrix for each given  $\mathbf{q}$ . Equation (17) has recently been derived by one of us [28], and its numerical solutions for  $E_3^{\text{be}}(\mathbf{q})$  are in excellent agreement with the DMRG simulations in a sawtooth lattice [27]. In particular, in sharp contrast with the exact results on the single-band linear-chain model which dismiss trimers [7,21,22,26], it is found that the presence of an additional band allows the formation of energetically stable trimer states in the sawtooth lattice. In addition, it is found that the trimers have a quasiflat dispersion when formed in a flat band, which is unlike the highly dispersive spectrum of its dimers. These surprising results are one of the main motivations for the current work, i.e., we want to study the stability of larger few-body clusters in the presence of multiple bands.

Let us next consider the four-body problem and study the fate of tetramer bound states. For  $N = 3$ , Eq. (14) reduces to

$$\begin{aligned} \gamma_{n_2 n_3 S}^{\mathbf{k}_2 \mathbf{k}_3}(\mathbf{q}) &= \frac{U}{N_c} \sum_{n_1 m S' \mathbf{k}_1} \frac{m_{S' \mathbf{Q} \downarrow}^* m_{S \mathbf{Q} \downarrow} n_{1 S \mathbf{k}_1 \uparrow}}{(\sum_{i=1}^3 \varepsilon_{n_i \mathbf{k}_i \uparrow}) + \varepsilon_{m \mathbf{Q} \downarrow} - E_4^{\mathbf{q}}} \\ &\times [n_{1 S' \mathbf{k}_1 \uparrow}^* \gamma_{n_2 n_3 S'}^{\mathbf{k}_2 \mathbf{k}_3}(\mathbf{q}) - n_{2 S' \mathbf{k}_2 \uparrow}^* \gamma_{n_1 n_3 S'}^{\mathbf{k}_1 \mathbf{k}_3}(\mathbf{q}) \\ &- n_{3 S' \mathbf{k}_3 \uparrow}^* \gamma_{n_2 n_1 S'}^{\mathbf{k}_2 \mathbf{k}_1}(\mathbf{q})], \end{aligned} \quad (18)$$

where  $\mathbf{Q} = \mathbf{q} - \mathbf{k}_1 - \mathbf{k}_2 - \mathbf{k}_3$ . This is a set of  $N_b^3$  coupled integral equations with two momentum variables, and it can be recast as an eigenvalue problem of an  $N_b^3 N_c^2 \times N_b^3 N_c^2$  matrix for each given  $\mathbf{q}$ . Our numerical recipe is provided in Appendix A. In this work, we apply Eqs. (16), (17), and (18) to the sawtooth model due in part to its flat band and one-dimensional simplicity, and most importantly to our benchmarking capacity with the DMRG simulations and exact diagonalization.

### III. SAWTOOTH LATTICE

Due to the presence of its  $N_b = 2$  sublattice sites in a unit cell (say  $S = \{A, B\}$  sublattices), the sawtooth lattice features two Bloch bands in the first BZ (say  $s = \{+, -\}$  bands). See the inset of Fig. 3(a) for its sketch, where  $a$  is the lattice spacing. Here we allow hopping between nearest-neighbor

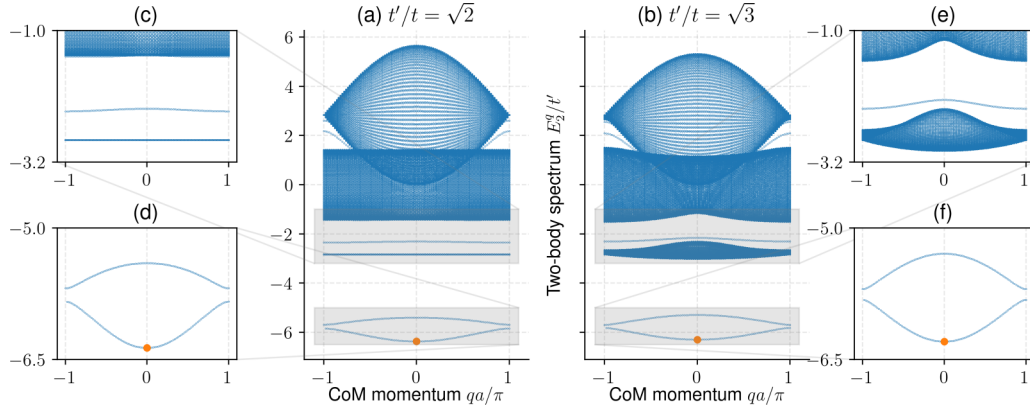


FIG. 1. Two-body spectrum  $E_2^q$  in a sawtooth lattice for  $t = t'/\sqrt{2}$  (left column) and  $t = t'/\sqrt{3}$  (right column), when  $U = 5t'$ . Insets (d) and (f) are zooms to the lower and upper on-site dimer branches. Insets (c) and (e) are zooms to the first and second monomer-monomer continua, and two distinct off-site dimer branches in between. In (c) the highly degenerate first continuum states appear precisely at  $-2\sqrt{2}t' \approx -2.83t'$ , and the lower off-site dimer branch is around  $-2.35t'$ . The upper off-site dimer branch is underneath the second continuum but it is not visible in this scale. Benchmarks with the DMRG ground states are shown with an orange-colored marker •.

sites only, and we set  $t_{Aj;Ai}^\sigma = -t$  with  $j = i \pm 1$  and  $t \geq 0$ ,  $t_{Bj;Bi}^\sigma = 0$  and  $t_{Bi;Ai}^\sigma = t_{Bj;Ai}^\sigma = -t'$  with  $j = i - 1$  and  $t' \geq 0$ . Thus the one-body Hamiltonian can be written as

$$\mathcal{H}_\sigma = \sum_k \psi_{k\sigma}^\dagger (d_k^0 \sigma_0 + \mathbf{d}_k \cdot \boldsymbol{\sigma}) \psi_{k\sigma}, \quad (19)$$

where  $\psi_{k\sigma} = (c_{Ak\sigma} \ c_{Bk\sigma})^T$  is a sublattice spinor;  $-\pi/a < k \leq \pi/a$  is in the first BZ,  $d_k^0 = t \cos(ka)$ ;  $\sigma_0$  is a  $2 \times 2$  identity matrix;  $\mathbf{d}_k = (d_k^x, d_k^y, d_k^z)$  is a field vector with elements  $d_k^x = t' + t' \cos(ka)$ ,  $d_k^y = t' \sin(ka)$ , and  $d_k^z = t \cos(ka)$ ; and  $\boldsymbol{\sigma} = (\sigma_x, \sigma_y, \sigma_z)$  is a vector of Pauli spin matrices. The one-body dispersions can be written as  $\varepsilon_{sk\sigma} = d_k^0 + sd_k$ , where  $s = \pm$  for the upper and lower bands, respectively, and  $d_k$  is the magnitude of  $\mathbf{d}_k$ . The sublattice projections of the corresponding eigenvectors are  $s_{Ak\sigma} = (-d_k^x + id_k^y)/\sqrt{2d_k(d_k - sd_k^z)}$  and  $s_{Bk\sigma} = (d_k^z - sd_k)/\sqrt{2d_k(d_k - sd_k^z)}$ . One of the most treasured features of this toy model is the presence of a flat (lower) band  $\varepsilon_{-,k} = -2t$  in its dispersion when  $t'/t = \sqrt{2}$  [27,28,50–53].

### A. Full (1 + 1)-body spectrum

Equation (16) determines only the two lowest-energy dimer bound states [27,28,45,46]. To reveal the full two-body spectrum, one may recast Eq. (16) as an eigenvalue problem in terms of the original variational parameters,

$$0 = (\varepsilon_{n_1\mathbf{k}_1\uparrow} + \varepsilon_{n_2,\mathbf{q}-\mathbf{k}_1,\downarrow} - E_2^q) \alpha_{n_1 n_2}^{\mathbf{k}_1}(\mathbf{q}) - \frac{U}{N_c} \sum_{n'_1 n'_2 \mathbf{k}_S} n_{1S\mathbf{k}_1\uparrow}^* \times n_{2S,\mathbf{q}-\mathbf{k}_1,\downarrow}^* n'_{1S\mathbf{k}_\uparrow} n'_{2S,\mathbf{q}-\mathbf{k}_1,\downarrow} \alpha_{n'_1 n'_2}^{\mathbf{k}}(\mathbf{q}), \quad (20)$$

and solve for  $E_2^q$  [45]. This can be achieved by further recasting it as an eigenvalue problem using an  $N_b^2 N_c \times N_b^2 N_c$  matrix for each given  $\mathbf{q}$ . Here we use a  $k$ -space mesh with  $N_c = 100$  points for the two-body problem.

Our two-body spectra are shown in Fig. 1 for  $t'/t = \{\sqrt{2}, \sqrt{3}\}$  when  $U = 5t'$ . At the bottom of each spectrum, there are two distinct bound states for a given  $q$ . We refer to them as the on-site dimer states (they are also referred

to as doublons [27]) since their binding energy grows with  $U$  without a limit, i.e., the two monomers are eventually tightly bound and they are strongly colocalized on one site in the strong-coupling limit. They are shown in Figs. 1(d) and 1(f). Above the on-site dimers, there are the first monomer-monomer continuum states, corresponding to two unbound monomers that occupy the lower Bloch band. Note that there is a continuum of highly degenerate states at energy  $-2\sqrt{2}t' \approx -2.83t'$  in the flat-band case shown in Fig. 1(c), i.e., when  $t'/t = \sqrt{2}$ . The next monomer-monomer continuum states correspond to two unbound monomers that occupy the lower and upper Bloch bands one at a time. In between the first and second continuum there are also the so-called off-site dimer bound states. There are two of them, but the upper one is barely visible since it is very close to the bottom of the second continuum. Unlike those of the on-site dimers, the binding energy of the off-site dimers saturates with  $U$ , i.e., the two monomers are weakly bound no matter what  $U$  is. The closest the two monomers can get is on nearest-neighbor sites in the strong-coupling limit. The third monomer-monomer continuum states correspond to two unbound monomers that occupy the upper Bloch band. In between the second and third continuum there also appears two weakly bound off-site dimer bound states near the edges of the BZ. Thus we conclude that the off-site dimer states are a multiband phenomenon, and they emerge in between every two consecutive monomer-monomer continua.

We note that the presence of a flat Bloch band does not have much of an impact on the dispersion of the on-site dimers. This is because the diverging bare effective band mass of the flat-band monomers gets dressed by the interband transitions, which produce a finite effective band mass for the on-site dimers at any  $U \neq 0$ . This somewhat counterintuitive effect is well-studied in the recent literature in the context of quantum geometry [45,46]. See also Ref. [27] for the sawtooth lattice. The effective band mass of the on-site dimers makes a dip in the weak-coupling regime, and then it increases for stronger couplings, leading to a more and more localized on-site dimer in space. This is because an on-site dimer is allowed to hop in the Hubbard model through the so-called virtual ionization,

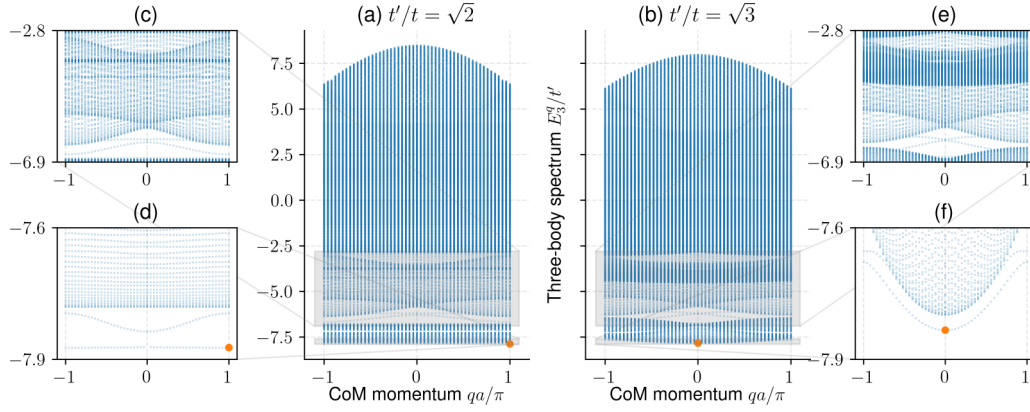


FIG. 2. Three-body spectrum  $E_3^q$  in a sawtooth lattice for  $t = t'/\sqrt{2}$  (left column) and  $t = t'/\sqrt{3}$  (right column) when  $U = 5t'$ . Insets (d) and (f) are zooms to the off-site trimer branches and the first and second dimer-monomer continua above them. Insets (c) and (e) are zooms to the excited off-site trimer branches and the third and fourth dimer-monomer continua above them. In (c) there is also a highly degenerate first monomer-monomer-monomer continuum of states appearing precisely at  $-3\sqrt{2}t' \approx -4.24t'$ , and the origin of the continuum of states around  $-2.35t' - \sqrt{2}t' \approx -3.76t'$  can be traced back to the lower off-site dimer branch shown in Fig. 1(c). Benchmarks with the DMRG ground states are shown with orange-colored markers •.

and this brings a factor of  $1/E_2^{\text{be}}(\mathbf{0})$  as a punishment from second-order perturbation theory. On the other hand, the off-site dimers have a negligible dispersion when they form in a flat band, e.g., in Fig. 1(c). This is because their effective band mass is largely controlled by the bare effective band mass of the weakly bound monomers.

### B. Full $(2 + 1)$ -body spectrum

Equation (17) can be used to calculate the energy of the ground-state trimers through an iterative procedure [28]. However, in order to reveal the full three-body spectrum, we recast Eq. (17) as an eigenvalue problem in terms of the original variational parameters,

$$\begin{aligned}
 0 = & (\varepsilon_{n_1\mathbf{k}_1\uparrow} + \varepsilon_{n_2\mathbf{k}_2\uparrow} + \varepsilon_{n_3\mathbf{Q}\downarrow} - E_3^q) \alpha_{n_1n_2n_3}^{\mathbf{k}_1\mathbf{k}_2}(\mathbf{q}) \\
 & - \frac{U}{2N_c} \sum_{n'_1n'_3\mathbf{k}\mathbf{S}} n_{1S\mathbf{k}_1\uparrow}^* n_{3S\mathbf{Q}\downarrow}^* n'_{3S,\mathbf{q}-\mathbf{k}_2-\mathbf{k},\downarrow} n'_{1S\mathbf{k}} \alpha_{n'_1n'_2n'_3}^{\mathbf{k}\mathbf{k}_2}(\mathbf{q}) \\
 & - \frac{U}{2N_c} \sum_{n'_2n'_3\mathbf{k}\mathbf{S}} n_{2S\mathbf{k}_2\uparrow}^* n_{3S\mathbf{Q}\downarrow}^* n'_{3S,\mathbf{q}-\mathbf{k}_1-\mathbf{k},\downarrow} n'_{2S\mathbf{k}} \alpha_{n'_1n'_2n'_3}^{\mathbf{k}_1\mathbf{k}}(\mathbf{q}) \\
 & + \frac{U}{2N_c} \sum_{n'_2n'_3\mathbf{k}\mathbf{S}} n_{1S\mathbf{k}_1\uparrow}^* n_{3S\mathbf{Q}\downarrow}^* n'_{3S,\mathbf{q}-\mathbf{k}_2-\mathbf{k},\downarrow} n'_{2S\mathbf{k}} \alpha_{n'_2n'_2n'_3}^{\mathbf{k}_2\mathbf{k}}(\mathbf{q}) \\
 & + \frac{U}{2N_c} \sum_{n'_1n'_3\mathbf{k}\mathbf{S}} n_{2S\mathbf{k}_2\uparrow}^* n_{3S\mathbf{Q}\downarrow}^* n'_{3S,\mathbf{q}-\mathbf{k}_1-\mathbf{k},\downarrow} n'_{1S\mathbf{k}} \alpha_{n'_1n'_1n'_3}^{\mathbf{k}\mathbf{k}_1}(\mathbf{q}),
 \end{aligned} \tag{21}$$

and we solve for  $E_3^q$ . Recall that  $\mathbf{Q} = \mathbf{q} - \mathbf{k}_1 - \mathbf{k}_2$  when  $N = 2$ , and note that the exchange-symmetry constraints are imposed on the variational parameters by construction. This can be achieved by further recasting it as an eigenvalue problem using an  $N_b^3 N_c^2 \times N_b^3 N_c^2$  matrix for each given  $\mathbf{q}$ . Here we use a  $k$ -space mesh with  $N_c = 50$  points for the three-body problem. The numerical procedure is similar to the one given in Appendix A.

Our three-body spectra are shown in Fig. 2 for  $t'/t = \{\sqrt{2}, \sqrt{3}\}$  when  $U = 5t'$ . See also Fig. 7 in Appendix C for

similar results when  $U = 10t'$ , where some of the features discussed below are more visible. At the bottom of each spectrum, there are typically two distinct bound-state solutions for a given  $q$ . Here we refer to both of them as the off-site trimer states since their binding energies again saturate with  $U$ . They are shown in Figs. 2(d) and 2(f). The lower trimer branch is in perfect agreement with the recent literature [27,28]. These trimers consist of a dimer that is strongly localized on one site and a monomer on another site even in the strong-coupling limit, i.e., the closest the dimer and the monomer can be is on nearest-neighbor sites. See also our remarks in Sec. III D for their binding mechanism. Note that the trimer bound states are necessarily off-site and they are weakly bound due to the Pauli exclusion principle preventing the formation of on-site trimers. Above the off-site trimers, there are the first dimer-monomer continuum states, corresponding to two monomers occupying the lower on-site dimer branch and a monomer occupying the lower Bloch band. The next dimer-monomer continuum states correspond to two monomers in the upper on-site dimer branch and a monomer in the lower Bloch band. In the flat-band case, we note that the energy gap between these dimer-monomer continua corresponds exactly to the energy gap between the on-site dimer branches shown in Fig. 1(d). Within this energy gap there also appears a barely visible off-site trimer bound state beneath the second continuum. The third dimer-monomer continuum states correspond to two monomers in the lower on-site dimer branch and a monomer in the upper Bloch band, and the fourth dimer-monomer continuum corresponds to two monomers in the upper on-site dimer branch and a monomer in the upper Bloch band. In between the second and third dimer-monomer continuum, there appears three weakly bound off-site trimer states. They are shown in Figs. 2(c) and 2(e). All of the monomer-monomer-monomer continuum states, corresponding to three unbound monomers occupying various combinations of the upper and lower Bloch bands, appear mixed together. For instance, there is a continuum of highly degenerate states at energy  $-3\sqrt{2}t' \approx -4.24t'$  in the flat-band case shown in Fig. 2(c), which comes from three monomers occupying the

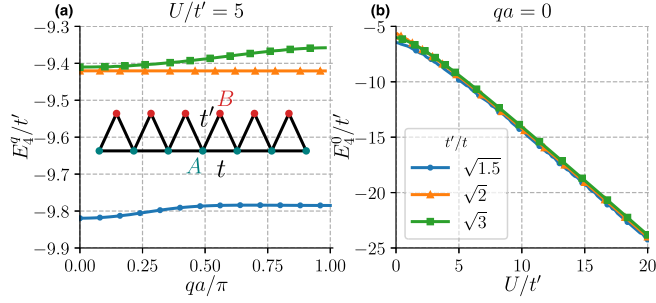


FIG. 3. Lowest-lying tetramer energies from the variational approach. In (a) the tetramer dispersion is quasiflat when they form in a flat band, i.e., when  $t'/t = \sqrt{2}$ . Note that the sawtooth lattice is sketched in the inset of (a).

lower Bloch band. The next continuum that consists of two monomers in the lower Bloch band and a monomer in the upper Bloch band clearly starts at  $-2\sqrt{2}t' \approx -2.83t'$ . The origin of the continuum of states around  $-2.35t' - \sqrt{2}t' \approx -3.76t'$  can be traced back to the occupation of the lower off-site dimer branch shown in Fig. 1(c) by two monomers along with a monomer in the lower Bloch band.

### C. Ground-state tetramers

Here we analyze the ground state of the  $(3+1)$ -body problem. See Appendix A for its numerical implementation. Our variational results for the  $E_4^q$  and  $E_4^0$  are presented, respectively, in Figs. 3(a) and 3(b), where we use a  $k$ -space mesh with  $N_c = 30$  points and we checked that using  $N_c = 50$  points makes minor corrections. Indeed, the ground-state energy of the tetramers is typically within 1% relative accuracy of the DMRG simulations (see below). One of our main findings is that the four-body dispersion  $E_4^q$  is quasiflat (with a negligible bandwidth) when the tetramers form in a flat band, i.e., when  $t'/t = \sqrt{2}$ . For instance, the  $U = 5t'$  case is shown in Fig. 3(a), and we found similar results for lower and higher  $U/t'$  values as well (not shown). It is conceivable that the tetramers have a respectable dispersion in the weak-coupling limit when  $U/t' \lesssim 1$ , but our numerical calculations are not expected to be as reliable there. This is because one needs to use a much higher  $N_c$  as the size of the bound states (in real space) gets much larger in the  $U/t' \rightarrow 0$  limit. We also calculated the binding energy  $E_4^{\text{be}}(q)$  of the tetramers and verified their energetic stability, e.g., we found that  $E_4^{\text{be}}(q)$  becomes positive as soon as  $U \neq 0$  when the tetramers form in a flat band. However, this is not the case when  $t'/t \neq \sqrt{2}$ , i.e.,  $E_4^{\text{be}}(q)$  becomes positive beyond a critical threshold on  $U$  in such a way that larger deviations from the flat-band case lead to a higher threshold.

### D. Ground-state pentamers and beyond

For  $N \geq 4$  it is possible to solve Eq. (14) again by recasting it as an eigenvalue problem, but such a numerically expensive task is beyond our capacity. Instead, here we present our numerical results from the DMRG simulations [54–56] and exact diagonalization [57]. For this purpose, we define the ground-state binding energy of the  $(N+1)$ -body bound

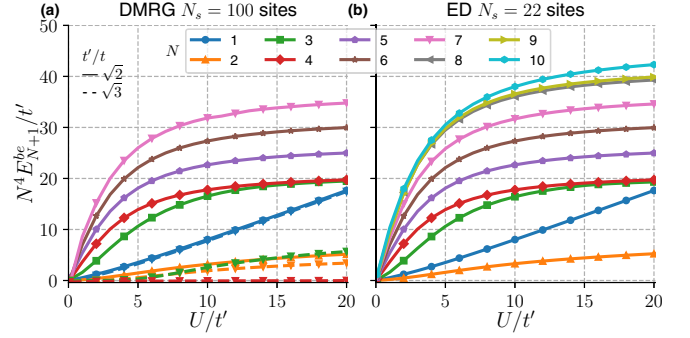


FIG. 4. (a) Binding energies  $E_{N+1}^{\text{be}}(\text{gs})$  from DMRG with  $N_s = 100$  sites for  $t'/t = \sqrt{2}$  (solid lines) and  $t'/t = \sqrt{3}$  (dashed lines). When  $N \geq 5$ , the multimers are not energetically stable for  $t'/t = \sqrt{3}$ , i.e.,  $E_{N+1}^{\text{be}}(\text{gs}) \leq 0$  (not shown). (b)  $E_{N+1}^{\text{be}}(\text{gs})$  from exact diagonalization with  $N_s = 22$  sites for  $t'/t = \sqrt{2}$ . Since  $E_{N+1}^{\text{be}}(\text{gs})$  decays rapidly with  $N$ , energies are multiplied with  $N^4$  in both figures for convenience.

state as

$$E_{N+1}^{\text{be}}(\text{gs}) = -E_0(N, 1) + E_0(N-1, 1) + E_0(1, 0), \quad (22)$$

where  $E_0(N_\uparrow, N_\downarrow)$  is the ground-state energy of the  $(N_\uparrow + N_\downarrow)$ -body problem. Given the definition in Eq. (15), Eq. (22) is strictly valid under the assumption that the COM momentum of the ground state of the  $(N+1)$ -body problem is equal to the total momentum of the ground states of the  $[(N-1)+1]$ -body and one-body problems. Unlike the  $t'/t < \sqrt{2}$  case, where the ground state of the one-body problem is at the edge of the BZ, our variational results suggest that this requirement is usually fulfilled when  $t'/t \geq \sqrt{2}$ .

In Fig. 4(a) we set  $t'/t = \{\sqrt{2}, \sqrt{3}\}$ , and we present the DMRG results for  $E_{N+1}^{\text{be}}(\text{gs})$  as a function of  $U/t'$ . Here we use a long lattice with  $N_s = 100$  sites and with open boundary conditions. We only show  $N = \{1, 2, \dots, 7\}$  since the accuracy of our DMRG simulations does not allow us to resolve  $E_{N+1}^{\text{be}}(\text{gs})$  for the entire  $U/t'$  range when  $N \geq 8$ . To overcome this limitation, we also perform the exact diagonalization of a fairly large lattice with  $N_s = 22$  sites, and they are presented in Fig. 4(b) for  $N = \{1, 2, \dots, 10\}$ . First of all, the variational, DMRG, and exact diagonalization approaches are in very good agreement with each other when they have an overlap at low  $N$  values. For  $N \geq 2$  they suggest the presence of larger and larger few-body clusters with lower and lower binding energies, conceivably without an upper bound on  $N$ . In addition, all of these clusters are energetically stable when formed in a flat band, i.e.,  $E_{N+1}^{\text{be}}(\text{gs}) > 0$  as soon as  $U \neq 0$ . Unlike  $E_2^{\text{be}}(\text{gs})$  of the dimer that grows linearly with  $U$  in the strong-coupling limit when  $U/t' \gg 1$ , we note that  $E_{N+1}^{\text{be}}(\text{gs})$  always saturates for  $N \geq 2$ , i.e., it fits quite well with  $C'_N t' - C''_N t'^2/U$ , where  $C'_N$  and  $C''_N$  both decay rapidly with  $N$ . These fits are shown in Fig. 5. In addition, we also checked the energies of the first few excited states in our exact diagonalization studies. As shown in Fig. 6 in Appendix B, the energy gaps between the first few excited states and the ground state vanish exactly when  $t'/t = \sqrt{2}$ . Thus it is also conceivable that some of the lowest-lying  $(N+1)$ -body bound states have quasiflat dispersions in the BZ when formed in a flat band.

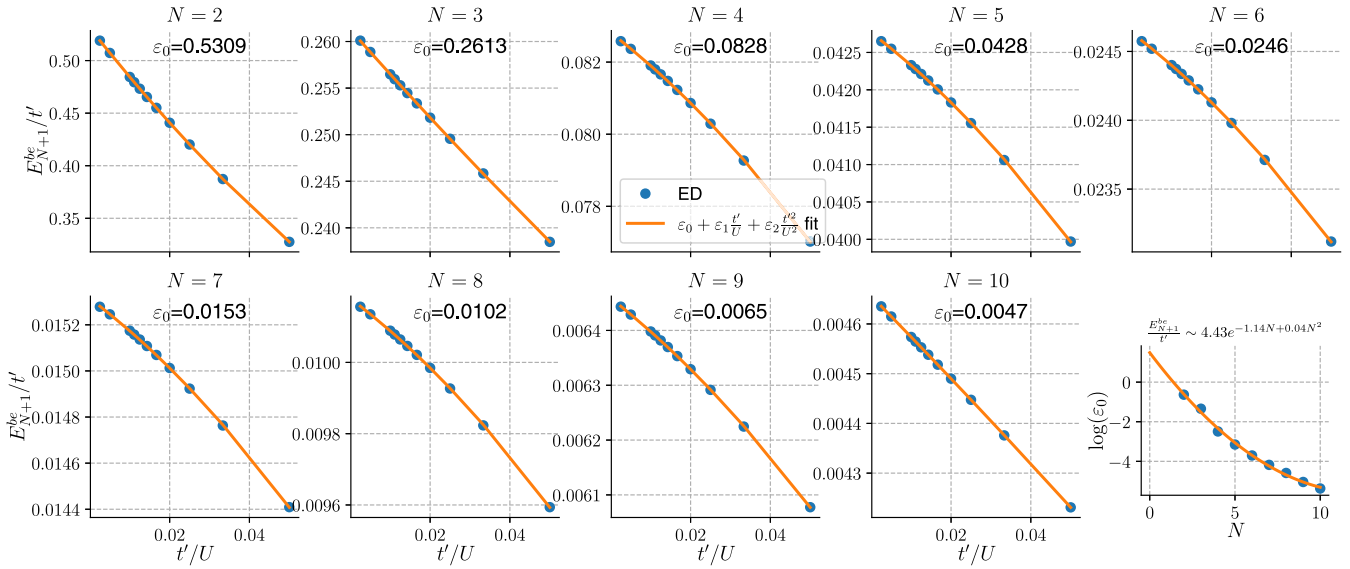


FIG. 5. Binding energies  $E_{N+1}^{be}$  (gs) from exact diagonalization with  $N_s = 22$  sites for  $t'/t = \sqrt{2}$ . The strong-coupling limit  $t'/U \ll 1$  seems to fit quite well with  $E_{N+1}^{be}(\text{gs})/t' = \epsilon_0 + \epsilon_1(t'/U) + \epsilon_2(t'/U)^2$  for all  $N \geq 2$ , where the saturation point  $\epsilon_0$  at  $t'/U \rightarrow 0$  decreases rapidly with  $N$ . It is also shown that the fit  $\epsilon_0 \sim 4.43e^{-1.14N+0.04N^2}$  matches reasonably well with the available data for  $N = \{2, 3, \dots, 10\}$ .

A plausible mechanism for the appearance of energetically stable  $(N + 1)$ -body bound states in a flat band is as follows: when the spin- $\uparrow$  fermions are strongly localized on the nonoverlapping localized states (thanks to their diverging effective band mass), the delocalization of the spin- $\downarrow$  fermion on these nearest-neighbor states might be favored by the on-site attraction in between. See Appendix B for a related numerical observation and more about localized states. This mechanism is analogous to the band formation for a single particle in a periodic potential, and the mobility of a spin- $\downarrow$  fermion can be achieved through interband transitions with the upper band, reducing the overall energy of the system. We note that a similar interband mechanism (that is mediated by  $U \neq 0$ )

is fully responsible for the finite effective mass of the low-energy dimers when they form in a flat band [27,45,46,49]. In this scenario, the spin- $\downarrow$  fermion can hop between spin- $\uparrow$  fermions only through dissociation of the virtual dimers, and this process leads to an effective hopping that scales as  $\sim C_N t'^2 / E_2^{be}(\text{gs})$ , where  $C_N$  depends on  $N$ . This further suggests that  $E_{N+1}^{be}(\text{gs}) \sim C'_N t' - C''_N t'^2 / U$  in the strong-coupling limit when  $U/t' \gg 1$  because  $E_2^{be}(\text{gs}) \rightarrow U$  in this limit. Indeed, this turns out to be the case in our exact diagonalization results that are shown in Fig. 5.

In the particular case of trimer bound states, this binding mechanism is in accordance with that revealed for the bosonic trimers (i.e., mediated by a particle-exchange interaction

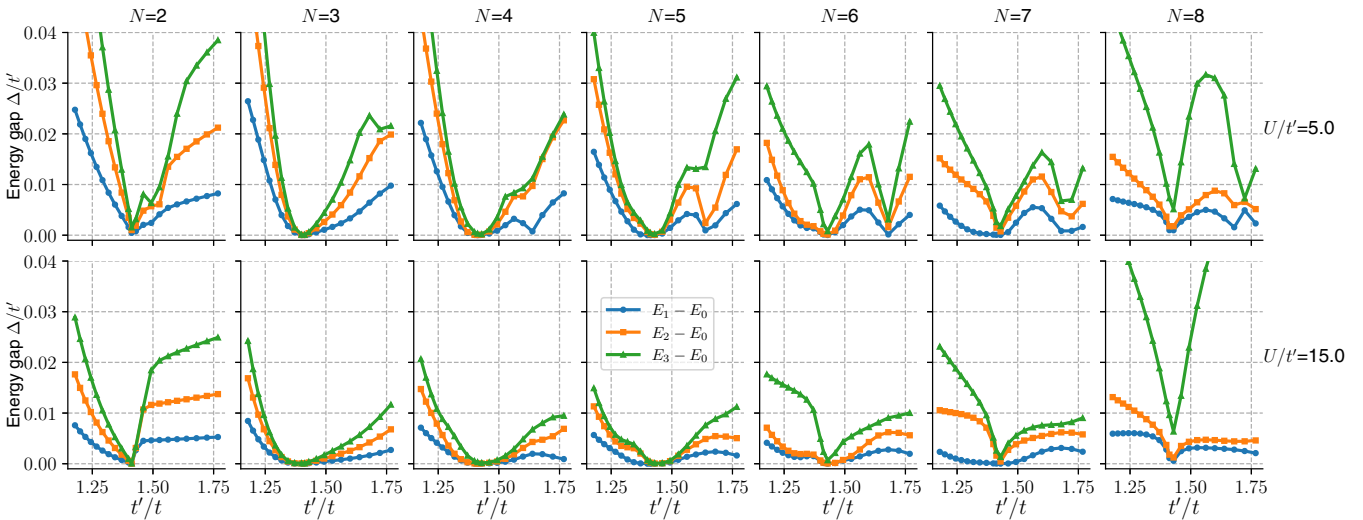


FIG. 6. Energy gaps from the exact diagonalization of a lattice with  $N_s = 22$  sites. Upper and lower panels correspond, respectively, to  $U/t' = 5$  and 15. In the flat-band case when  $t'/t = \sqrt{2}$ , large gaps appear once the number of  $\uparrow$  fermions ( $N$ ) exceeds the number of nonoverlapping localized states ( $N_s/4$ ), i.e., finite-size effects appear for  $N > N_s/4$ .

between the on-site dimer and the monomer) [58], and it has recently been studied through a perturbation theory in the strong-coupling limit [27]. Furthermore, given the fermion-boson mapping that is revealed in Appendix C, there is no doubt that the off-site fermion trimers are also bound through the very same mechanism in the strong-coupling limit.

#### IV. CONCLUSION

In summary, here we used variational, DMRG, and exact diagonalization approaches, and we studied the bound states of  $N$  identical spin- $\uparrow$  fermions and a single spin- $\downarrow$  fermion in a generic multiband Hubbard Hamiltonian with an attractive on-site interaction. In the case of a sawtooth lattice with a flat band, we showed strong evidence for the existence of energetically stable few-body clusters with  $N = \{2, 3, \dots, 10\}$ , conceivably without an upper bound on  $N$  and with a quasi-flat  $(N + 1)$ -body dispersion in the first BZ. These peculiar findings are in sharp contrast with the exact results on the single-band linear-chain model, which dismiss all of the  $N \geq 2$  multimers [7,21,22,26]. As an outlook, it is desirable to perform similar analyses for other toy models that exhibit flat bands in their spectrum, including, e.g., the kagomé and Lieb lattices [43]. Such analyses would help us uncover how versatile the critical role of a flat band is in the formation of few-body clusters, and how the induced attraction between the dimer and the rest of the fermions [16] arises through interband processes. In addition, one can easily extend our approach to study bound-state formation in a multiband Bose-Hubbard model [59].

#### ACKNOWLEDGMENTS

We thank M. Ö. Oktel for his comments and suggestions. A.K. is supported by TÜBİTAK 2236 Co-funded Brain Circulation Scheme 2 (CoCirculation2) Project No. 120C066.

#### APPENDIX A: NUMERICAL IMPLEMENTATION OF THE (3 + 1)-BODY PROBLEM

Equation (17) is a set of  $N_b^3$  coupled integral equations with two momentum variables, and here we show how to recast it as an eigenvalue problem using an  $N_b^3 N_c^2 \times N_b^3 N_c^2$  matrix for each given  $\mathbf{q}$ . The level of difficulty is the same as in the full spectrum of the  $(2 + 1)$ -body problem discussed in Sec. III B. We note that the full spectrum of the  $(3 + 1)$ -body spectrum is well beyond our moderate computation capacity. First we rewrite Eq. (17) as

$$\begin{aligned} \gamma_{nmS}^{\mathbf{kk}'}(\mathbf{q}) &= \sum_{S'} f_{nmS;nmS'}^{\mathbf{qkk}'} \gamma_{nmS'}^{\mathbf{kk}'}(\mathbf{q}) \\ &+ \sum_{n'm'S'p} g_{nmS;n'm'S'}^{\mathbf{qkk}'p} \gamma_{n'm'S'}^{\mathbf{pk}'}(\mathbf{q}) \\ &+ \sum_{n'm'S'p} h_{nmS;n'm'S'}^{\mathbf{qkk}'p} \gamma_{n'm'S'}^{\mathbf{kp}}(\mathbf{q}), \end{aligned} \quad (\text{A1})$$

whose coefficients  $f_{nmS;nmS'}^{\mathbf{qkk}'}$ ,  $g_{nmS;n'm'S'}^{\mathbf{qkk}'p}$ , and  $h_{nmS;n'm'S'}^{\mathbf{qkk}'p}$  are stored as

$$f_{nmS;nmS'}^{\mathbf{qkk}'} = \frac{U}{N_c} \sum_{n'm'p} \frac{m'^*_{S\mathbf{K}\downarrow} m'_{S\mathbf{K}\downarrow} n'_{S\mathbf{p}\uparrow} n'^*_{S'\mathbf{p}\uparrow}}{E_{nmn'm'}^{\mathbf{qkk}'p}}, \quad (\text{A2})$$

$$g_{nmS;n'm'S'}^{\mathbf{qkk}'p} = -\frac{U}{N_c} \frac{m'^*_{S'\mathbf{K}\downarrow} m'_{S\mathbf{K}\downarrow} n'_{S\mathbf{p}\uparrow} n'^*_{S'\mathbf{K}\uparrow}}{E_{nmn'm'}^{\mathbf{qkk}'p}}, \quad (\text{A3})$$

$$h_{nmS;n'm'S'}^{\mathbf{qkk}'p} = -\frac{U}{N_c} \frac{m'^*_{S'\mathbf{K}\downarrow} m'_{S\mathbf{K}\downarrow} n'_{S\mathbf{p}\uparrow} m'^*_{S'\mathbf{K}\uparrow}}{E_{nmn'm'}^{\mathbf{qkk}'p}}. \quad (\text{A4})$$

Here we defined  $\mathbf{K} = \mathbf{q} - \mathbf{k} - \mathbf{k}' - \mathbf{p}$  and  $E_{nmn'm'}^{\mathbf{qkk}'p} = \varepsilon_{n\mathbf{k}\uparrow} + \varepsilon_{m\mathbf{k}'\uparrow} + \varepsilon_{n'\mathbf{p}\uparrow} + \varepsilon_{m'\mathbf{K}\downarrow} - E_4^{\mathbf{q}}$  for convenience. Then we define an  $N_b^3$ -component vector, e.g.,

$$\boldsymbol{\gamma}_{\mathbf{kk}'}(\mathbf{q}) = [\gamma_{11A}^{\mathbf{kk}'}(\mathbf{q}) \quad \gamma_{11B}^{\mathbf{kk}'}(\mathbf{q}) \quad \gamma_{12A}^{\mathbf{kk}'}(\mathbf{q}) \quad \gamma_{12B}^{\mathbf{kk}'}(\mathbf{q}) \quad \gamma_{21A}^{\mathbf{kk}'}(\mathbf{q}) \quad \gamma_{21B}^{\mathbf{kk}'}(\mathbf{q}) \quad \gamma_{22A}^{\mathbf{kk}'}(\mathbf{q}) \quad \gamma_{22B}^{\mathbf{kk}'}(\mathbf{q})]^T \quad (\text{A5})$$

in the case of a lattice with two sublattice sites, i.e.,  $N_b = 2$ . Here  $n = \{1, 2\}$  is the band index,  $S = \{A, B\}$  is the sublattice index, and T is the transpose. Equation (A1) can be written as

$$\boldsymbol{\gamma}_{\mathbf{kk}'}(\mathbf{q}) = F_{\mathbf{q}}^{\mathbf{kk}'} \boldsymbol{\gamma}_{\mathbf{kk}'}(\mathbf{q}) + \sum_{\mathbf{p}} G_{\mathbf{q}}^{\mathbf{kk}'p} \boldsymbol{\gamma}_{\mathbf{pk}'}(\mathbf{q}) + \sum_{\mathbf{p}} H_{\mathbf{q}}^{\mathbf{kk}'p} \boldsymbol{\gamma}_{\mathbf{kp}}(\mathbf{q}), \quad (\text{A6})$$

where  $F_{\mathbf{q}}^{\mathbf{kk}'}$ ,  $G_{\mathbf{q}}^{\mathbf{kk}'p}$ , and  $H_{\mathbf{q}}^{\mathbf{kk}'p}$  are  $N_b^3 \times N_b^3$  matrices. For instance, in the case of a lattice with two sublattice sites, they are given by

$$F_{\mathbf{q}}^{\mathbf{kk}'} = \begin{pmatrix} f_{11A;11A}^{\mathbf{qkk}'} & f_{11A;11B}^{\mathbf{qkk}'} & 0 & 0 & 0 & 0 & 0 & 0 \\ f_{11B;11A}^{\mathbf{qkk}'} & f_{11B;11B}^{\mathbf{qkk}'} & 0 & 0 & 0 & 0 & 0 & 0 \\ 0 & 0 & f_{12A;12A}^{\mathbf{qkk}'} & f_{12A;12B}^{\mathbf{qkk}'} & 0 & 0 & 0 & 0 \\ 0 & 0 & f_{12B;12A}^{\mathbf{qkk}'} & f_{12B;12B}^{\mathbf{qkk}'} & 0 & 0 & 0 & 0 \\ 0 & 0 & 0 & 0 & f_{21A;21A}^{\mathbf{qkk}'} & f_{21A;21B}^{\mathbf{qkk}'} & 0 & 0 \\ 0 & 0 & 0 & 0 & f_{21B;21A}^{\mathbf{qkk}'} & f_{21B;21B}^{\mathbf{qkk}'} & 0 & 0 \\ 0 & 0 & 0 & 0 & 0 & 0 & f_{22A;22A}^{\mathbf{qkk}'} & f_{22A;22B}^{\mathbf{qkk}'} \\ 0 & 0 & 0 & 0 & 0 & 0 & f_{22B;22A}^{\mathbf{qkk}'} & f_{22B;22B}^{\mathbf{qkk}'} \end{pmatrix}, \quad (\text{A7})$$





$$\mathbb{G}_q = \left( \begin{array}{cccc|cccc|cccc|cccc} G_q^{k_1 k_1 k_1} & 0 & \dots & 0 & G_q^{k_1 k_1 k_2} & 0 & \dots & 0 & G_q^{k_1 k_1 k_3} & 0 & \dots & 0 & \dots & \dots \\ 0 & G_q^{k_1 k_2 k_1} & \dots & 0 & 0 & G_q^{k_1 k_2 k_2} & \dots & 0 & 0 & G_q^{k_1 k_2 k_3} & \dots & 0 & \dots & \dots \\ \vdots & \vdots & \ddots & \vdots & \vdots & \vdots & \ddots & \vdots & \vdots & \vdots & \ddots & \vdots & \vdots & \vdots \\ 0 & 0 & \dots & G_q^{k_1 k_{N_c} k_1} & 0 & 0 & \dots & G_q^{k_1 k_{N_c} k_2} & 0 & 0 & \dots & G_q^{k_1 k_{N_c} k_3} & \dots & \dots \\ \hline G_q^{k_2 k_1 k_1} & 0 & \dots & 0 & G_q^{k_2 k_1 k_2} & 0 & \dots & 0 & G_q^{k_2 k_1 k_3} & 0 & \dots & 0 & \dots & \dots \\ 0 & G_q^{k_2 k_2 k_1} & \dots & 0 & 0 & G_q^{k_2 k_2 k_2} & \dots & 0 & 0 & G_q^{k_2 k_2 k_3} & \dots & 0 & \dots & \dots \\ \vdots & \vdots & \ddots & \vdots & \vdots & \vdots & \ddots & \vdots & \vdots & \vdots & \ddots & \vdots & \vdots & \vdots \\ 0 & 0 & \dots & G_q^{k_2 k_{N_c} k_1} & 0 & 0 & \dots & G_q^{k_2 k_{N_c} k_2} & 0 & 0 & \dots & G_q^{k_2 k_{N_c} k_3} & \dots & \dots \\ \hline G_q^{k_3 k_1 k_1} & 0 & \dots & 0 & G_q^{k_3 k_1 k_2} & 0 & \dots & 0 & G_q^{k_3 k_1 k_3} & 0 & \dots & 0 & \dots & \dots \\ 0 & G_q^{k_3 k_2 k_1} & \dots & 0 & 0 & G_q^{k_3 k_2 k_2} & \dots & 0 & 0 & G_q^{k_3 k_2 k_3} & \dots & 0 & \dots & \dots \\ \vdots & \vdots & \ddots & \vdots & \vdots & \vdots & \ddots & \vdots & \vdots & \vdots & \ddots & \vdots & \vdots & \vdots \\ 0 & 0 & \dots & G_q^{k_3 k_{N_c} k_1} & 0 & 0 & \dots & G_q^{k_3 k_{N_c} k_2} & 0 & 0 & \dots & G_q^{k_3 k_{N_c} k_3} & \dots & \dots \\ \vdots & \vdots & \dots & \vdots & \vdots & \vdots & \dots & \vdots & \vdots & \vdots & \dots & \vdots & \vdots & \ddots \end{array} \right), \quad (\text{A13})$$

$$\mathbb{H}_q = \left( \begin{array}{cccc|cccc|cccc|cccc} H_q^{k_1 k_1 k_1} & H_q^{k_1 k_1 k_2} & \dots & H_q^{k_1 k_1 k_{N_c}} & 0 & 0 & \dots & 0 & 0 & 0 & \dots & 0 & 0 & \dots \\ H_q^{k_1 k_2 k_1} & H_q^{k_1 k_2 k_2} & \dots & H_q^{k_1 k_2 k_{N_c}} & 0 & 0 & \dots & 0 & 0 & 0 & \dots & 0 & 0 & \dots \\ \vdots & \vdots & \ddots & \vdots & \vdots & \vdots & \ddots & \vdots & \vdots & \vdots & \ddots & \vdots & \vdots & \ddots \\ H_q^{k_1 k_{N_c} k_1} & H_q^{k_1 k_{N_c} k_2} & \dots & H_q^{k_1 k_{N_c} k_{N_c}} & 0 & 0 & \dots & 0 & 0 & 0 & \dots & 0 & 0 & \dots \\ \hline 0 & 0 & \dots & 0 & H_q^{k_2 k_1 k_1} & H_q^{k_2 k_1 k_2} & \dots & H_q^{k_2 k_1 k_{N_c}} & 0 & 0 & \dots & 0 & 0 & \dots \\ 0 & 0 & \dots & 0 & H_q^{k_2 k_2 k_1} & H_q^{k_2 k_2 k_2} & \dots & H_q^{k_2 k_2 k_{N_c}} & 0 & 0 & \dots & 0 & 0 & \dots \\ \vdots & \vdots & \ddots & \vdots & \vdots & \vdots & \ddots & \vdots & \vdots & \vdots & \ddots & \vdots & \vdots & \ddots \\ 0 & 0 & 0 & 0 & H_q^{k_2 k_{N_c} k_1} & H_q^{k_2 k_{N_c} k_2} & \dots & H_q^{k_2 k_{N_c} k_{N_c}} & 0 & 0 & \dots & 0 & 0 & \dots \\ \hline 0 & 0 & \dots & 0 & 0 & 0 & \dots & 0 & H_q^{k_3 k_1 k_1} & H_q^{k_3 k_1 k_2} & \dots & \dots & \dots & \dots \\ 0 & 0 & \dots & 0 & 0 & 0 & \dots & 0 & H_q^{k_3 k_2 k_1} & H_q^{k_3 k_2 k_2} & \dots & \dots & \dots & \dots \\ \vdots & \vdots & \ddots & \vdots & \vdots & \vdots & \ddots & \vdots & \vdots & \vdots & \ddots & \vdots & \vdots & \ddots \end{array} \right). \quad (\text{A14})$$

Thus the four-body problem reduces to the solutions of an eigenvalue problem defined by Eq. (A11). It can be solved numerically by iterating  $E_4^q$  until one of the eigenvalues of  $\mathbb{F}^q + \mathbb{G}^q + \mathbb{H}^q$  becomes exactly 1. Typically there are many  $E_4^q$  solutions for a given set of lattice parameters. In this work, we are interested in those tetramer states with lowest energy for a given  $\mathbf{q}$ .

#### APPENDIX B: EXCITED STATES FROM THE EXACT DIAGONALIZATION

As shown in Fig. 6, the energy gaps between the first three excited states and the ground state vanish exactly at  $t'/t = \sqrt{2}$  for  $N = \{2, 3, 4, 5\}$ . On the other hand, when the number of  $\uparrow$  fermions  $N$  exceeds the number of nonoverlapping localized states in a flat band, one expects large energy gaps to appear due to finite-size effects. Here these gaps clearly appear for  $N \geq 6$ . To reveal their finite-size origin, we note that the localized one-body eigenstates, i.e.,  $\mathcal{H}_\sigma |LS\rangle_{i\sigma} = \varepsilon_{fb} |LS\rangle_{i\sigma}$ ,

associated with the flat band  $\varepsilon_{fb} = -2t$  in a sawtooth lattice can be written as [50,51]

$$|LS\rangle_{i\sigma} = \frac{1}{2} (\sqrt{2} c_{A i \sigma}^\dagger - c_{B i \sigma}^\dagger - c_{B, i-1, \sigma}^\dagger) |0\rangle. \quad (\text{B1})$$

By sketching these localized states on a lattice, one finds that there can be at most  $N_s/4 = N_c/2$  of them that are not overlapping in space. This is why larger and larger energy gaps appear for  $N \geq 6$  in our exact diagonalization calculations with  $N_s = 22$  sites. For this reason, one may think of these weakly bound  $(N+1)$ -body multimers as some sort of Wigner molecules that are caused by the occupation of these nonoverlapping localized states.

In light of these results, and assuming much larger lattices, it is conceivable that some of these  $(N+1)$ -body bound states have quasiflat dispersions when formed in a flat one-body band. It is important to remark here that the  $(N+1)$ -body bound states may not be energetically stable for all  $N$  when  $t'/t \neq \sqrt{2}$ ; see, e.g., Fig. 4(a) for the  $t'/t = \sqrt{3}$  case, where

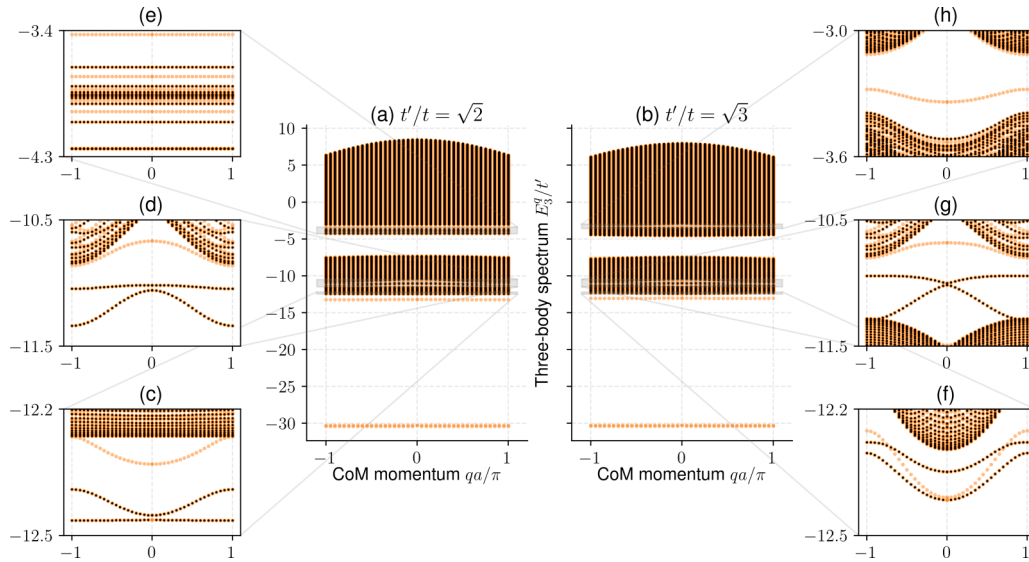


FIG. 7. Three-body spectrum  $E_3^q$  in a sawtooth lattice for  $t = t'/\sqrt{2}$  (left column) and  $t = t'/\sqrt{3}$  (right column) when  $U = 10t'$ . Here  $N_c = 40$  is chosen for better visibility. Fermion (boson) results are shown in black (yellow). The boson ground state is an on-site boson trimer with energy around  $-3U$ . There always exists an excited off-site boson trimer bound state for every off-site fermion trimer bound state with the same energy. In particular, insets (c) and (f) show that the ground state of the fermion trimer is on top of the fifth lowest eigenvalue (i.e., the third off-site boson trimer branch) of the boson trimer for any given COM momentum  $q$ .

$N \geq 5$  are not stable. To understand the origin of their quasi-flat dispersions, we note that the formation of tightly bound on-site trimers, on-site tetramers, etc., is prohibited by the Pauli exclusion principle. For this reason, the low-energy bound states of the  $(N + 1)$ -body problem are necessarily off-site, i.e., they consist of a dimer on one site and  $N - 1$  monomers on other sites in the strong-coupling limit. These off-site trimers, off-site tetramers, etc., have negligible dispersions when they form in a flat band because their effective band masses are largely controlled by the bare effective band masses of the dimer and infinitely massive monomers, as they are weakly bound. That is, the effective band mass of any off-site multimer is approximately given by the bare effective band mass of the dimer and the uncoupled monomers.

### APPENDIX C: FERMION-BOSON MAPPING IN THE THREE-BODY PROBLEM

It turns out the off-site  $(2 + 1)$ -body fermion trimers that we presented in Sec. III B for the low-energy bound states of the multiband attractive Hubbard model are in many ways similar to the off-site boson trimers that we recently reported for the excited bound states of the multiband attractive Bose-Hubbard model [59]. For instance, similar to the off-site dimers, the off-site fermion and off-site boson trimers both have negligible dispersions when they form in a flat band. This is because their effective band masses are largely controlled by the effective band masses of the infinitely massive monomer and the dimer, as the two are weakly bound. What is striking is that, in the case of the sawtooth model, the low-energy spectrum of the  $(2 + 1)$ -body fermion problem coincides exactly (i.e., up to machine precision) with excited states of the three-boson problem. Our variational calculations show that this is generally the case for any given set of  $\{t/t', U/t'\}$ , and we illustrate them in Fig. 7. The spectra

are such that the energy of the ground fermion trimer state coincides with the fifth lowest eigenvalue (i.e., the third off-site boson trimer branch) of the boson one for any given COM momentum  $q$ . In addition, the energy of the excited fermion trimer state coincides with the seventh lowest eigenvalue (i.e., the fifth off-site boson trimer branch) of the boson one.

Note that at the bottom of the three-boson spectrum there are also two distinct bound-state solutions for a given  $q$  [59]. They look degenerate in this scale with energies around  $-3U$ . These are referred to as the on-site boson trimer states since their binding energy grows with  $U$  without a limit, i.e., the three monomers are eventually tightly bound and they are strongly colocalized on one site in the strong-coupling limit. Unlike the highly dispersive on-site dimers (recall that the two-boson spectrum is identical to that of the two-fermion one discussed in Sec. III A), the on-site trimers have nearly flat dispersions even in the weak-binding low- $U/t'$  regime. This is because an on-site trimer is allowed to hop in the Bose-Hubbard model through the so-called virtual ionization, and this brings a factor of  $1/U^2$  as punishment from third-order perturbation theory. Since the effective band mass of the on-site trimers is much larger in magnitude than that of the on-site dimers, the on-site trimers are more localized in space.

The binding mechanism for the on-site boson trimers is very different from that of the off-site boson trimers. The binding mechanism for the strongly bound on-site trimers (and for all other on-site multimers for that matter) is trivial and obvious: similar to the on-site dimer case, the monomers are directly bound by the on-site attraction term that is present in the Hamiltonian. On the other hand, the binding mechanism for the weakly bound off-site trimers (and for off-site dimers and all other off-site multimers for that matter) is far less obvious: the binding is mediated by a peculiar particle-exchange interaction between the on-site dimer and the monomer on

nearest-neighbor sites [58]. The mediated interaction depends only on the hopping parameters  $t/t'$  but not on  $U/t'$ . This is why the binding energy of the off-site boson trimers saturates in the strong-coupling limit. Furthermore, given the fermion-boson mapping that is illustrated in Fig. 7, there is no

doubt that the off-site fermion trimers are also bound through the very same mechanism. This explains why their binding energy also saturates in the strong-coupling limit. Indeed, this mechanism has recently been studied through a perturbation theory in the strong-coupling limit [27].

- 
- [1] E. Braaten and H.-W. Hammer, Universality in few-body systems with large scattering length, *Phys. Rep.* **428**, 259 (2006).
- [2] H.-W. Hammer and L. Platter, Efimov states in nuclear and particle physics, *Annu. Rev. Nucl. Part. Sci.* **60**, 207 (2010).
- [3] D. Blume, Few-body physics with ultracold atomic and molecular systems in traps, *Rep. Prog. Phys.* **75**, 046401 (2012).
- [4] C. H. Greene, P. Giannakeas, and J. Pérez-Ríos, Universal few-body physics and cluster formation, *Rev. Mod. Phys.* **89**, 035006 (2017).
- [5] P. Naidon and S. Endo, Efimov physics: A review, *Rep. Prog. Phys.* **80**, 056001 (2017).
- [6] J. P. D’Incao, Few-body physics in resonantly interacting ultracold quantum gases, *J. Phys. B* **51**, 043001 (2018).
- [7] D. C. Mattis, The few-body problem on a lattice, *Rev. Mod. Phys.* **58**, 361 (1986).
- [8] T. Kraemer, M. Mark, P. Waldburger, J. G. Danzl, C. Chin, B. Engeser, A. D. Lange, K. Pilch, A. Jaakkola, H.-C. Nägerl, and R. Grimm, Evidence for Efimov quantum states in an ultracold gas of caesium atoms, *Nature (London)* **440**, 315 (2006).
- [9] M. Zaccanti, B. Deissler, C. D’Errico, M. Fattori, M. Jonas, S. Müller, G. Roati, M. Inguscio, and G. Modugno, Observation of an Efimov spectrum in an atomic system, *Nat. Phys.* **5**, 586 (2009).
- [10] S. E. Pollack, D. Dries, and R. G. Hulet, Universality in three- and four-body bound states of ultracold atoms, *Science* **326**, 1683 (2009).
- [11] N. Gross, Z. Shotan, S. Kokkelmans, and L. Khaykovich, Observation of Universality in Ultracold  $^7\text{Li}$  Three-Body Recombination, *Phys. Rev. Lett.* **103**, 163202 (2009).
- [12] R. Grimm, Efimov states in an ultracold gas: How it happened in the laboratory, *Few-Body Syst.* **60**, 23 (2019).
- [13] O. I. Kartavtsev and A. V. Malykh, Low-energy three-body dynamics in binary quantum gases, *J. Phys. B* **40**, 1429 (2007).
- [14] Y. Castin, C. Mora, and L. Pricoupenko, Four-Body Efimov Effect for Three Fermions and a Lighter Particle, *Phys. Rev. Lett.* **105**, 223201 (2010).
- [15] J. Levinsen and M. M. Parish, Bound States in a Quasi-Two-Dimensional Fermi Gas, *Phys. Rev. Lett.* **110**, 055304 (2013).
- [16] M. Jag, M. Zaccanti, M. Cetina, R. S. Lous, F. Schreck, R. Grimm, D. S. Petrov, and J. Levinsen, Observation of a Strong Atom-Dimer Attraction in a Mass-Imbalanced Fermi-Fermi Mixture, *Phys. Rev. Lett.* **112**, 075302 (2014).
- [17] D. Blume, Universal Four-Body States in Heavy-Light Mixtures with a Positive Scattering Length, *Phys. Rev. Lett.* **109**, 230404 (2012).
- [18] B. Bazak and D. S. Petrov, Five-Body Efimov Effect and Universal Pentamer in Fermionic Mixtures, *Phys. Rev. Lett.* **118**, 083002 (2017).
- [19] A. Sanayei, P. Naidon, and L. Mathey, Electron trimer states in conventional superconductors, *Phys. Rev. Research* **2**, 013341 (2020).
- [20] R. Liu, C. Peng, and X. Cui, Universal Tetramer and Pentamer in Two-dimensional Fermionic Mixtures, *Phys. Rev. Lett.* **129**, 073401 (2022).
- [21] G. Orso, E. Burovski, and T. Jolicoeur, Luttinger Liquid of Trimers in Fermi Gases with Unequal Masses, *Phys. Rev. Lett.* **104**, 065301 (2010).
- [22] G. Orso, E. Burovski, and T. Jolicoeur, Fermionic trimers in spin-dependent optical lattices, *C. R. Phys.* **12**, 39 (2011).
- [23] G. Roux, E. Burovski, and T. Jolicoeur, Multimer formation in one-dimensional two-component gases and trimer phase in the asymmetric attractive Hubbard model, *Phys. Rev. A* **83**, 053618 (2011).
- [24] M. Dalmonte, K. Dieckmann, T. Roscilde, C. Hartl, A. E. Feiguin, U. Schollwöck, and F. Heidrich-Meisner, Dimer, trimer, and Fulde-Ferrell-Larkin-Ovchinnikov liquids in mass- and spin-imbalanced trapped binary mixtures in one dimension, *Phys. Rev. A* **85**, 063608 (2012).
- [25] A. Dhar, P. Törmä, and J. J. Kinnunen, Fast trimers in a one-dimensional extended Fermi-Hubbard model, *Phys. Rev. A* **97**, 043624 (2018).
- [26] M. Takahashi, Excitonic insulator in one dimension, *Prog. Theor. Phys.* **43**, 917 (1970).
- [27] G. Orso and M. Singh, Pairs, trimers, and bcs-bec crossover near a flat band: Sawtooth lattice, *Phys. Rev. B* **106**, 014504 (2022).
- [28] M. Iskin, Three-body problem in a multiband Hubbard model, *Phys. Rev. A* **105**, 063310 (2022).
- [29] G.-B. Jo, J. Guzman, C. K. Thomas, P. Hosur, A. Vishwanath, and D. M. Stamper-Kurn, Ultracold Atoms in a Tunable Optical Kagome Lattice, *Phys. Rev. Lett.* **108**, 045305 (2012).
- [30] Y. Nakata, T. Okada, T. Nakanishi, and M. Kitano, Observation of flat band for terahertz spoof plasmons in a metallic kagome lattice, *Phys. Rev. B* **85**, 205128 (2012).
- [31] Z. Li, J. Zhuang, L. Wang, H. Feng, Q. Gao, X. Xu, W. Hao, X. Wang, C. Zhang, K. Wu, S. X. Dou, L. Chen, Z. Hu, and Y. Du, Realization of flat band with possible nontrivial topology in electronic kagome lattice, *Sci. Adv.* **4**, eaau4511 (2018).
- [32] F. Diebel, D. Leykam, S. Kroesen, C. Denz, and A. S. Desyatnikov, Conical Diffraction and Composite Lieb Bosons in Photonic Lattices, *Phys. Rev. Lett.* **116**, 183902 (2016).
- [33] S. Kajiwara, Y. Urade, Y. Nakata, T. Nakanishi, and M. Kitano, Observation of a nonradiative flat band for spoof surface plasmons in a metallic Lieb lattice, *Phys. Rev. B* **93**, 075126 (2016).
- [34] H. Ozawa, S. Taie, T. Ichinose, and Y. Takahashi, Interaction-Driven Shift and Distortion of a Flat Band in an Optical Lieb Lattice, *Phys. Rev. Lett.* **118**, 175301 (2017).
- [35] M. R. Slot, T. S. Gardenier, P. H. Jacobse, G. C. van Miert, S. N. Kempkes, S. J. Zevenhuizen, C. M. Smith, D. Vanmaekelbergh, and I. Swart, Experimental realization and characterization of an electronic Lieb lattice, *Nat. Phys.* **13**, 672 (2017).

- [36] M. N. Huda, S. Kezilebieke, and P. Liljeroth, Designer flat bands in quasi-one-dimensional atomic lattices, *Phys. Rev. Research* **2**, 043426 (2020).
- [37] D. P. Arovas, E. Berg, S. A. Kivelson, and S. Raghu, The Hubbard model, *Annu. Rev. Condens. Matter Phys.* **13**, 239 (2022).
- [38] S. A. Parameswaran, R. Roy, and S. L. Sondhi, Fractional quantum hall physics in topological flat bands, *C. R. Phys.* **14**, 816 (2013).
- [39] Z. Liu, F. Liu, and Y.-S. Wu, Exotic electronic states in the world of flat bands: From theory to material, *Chin. Phys. B* **23**, 077308 (2014).
- [40] D. Leykam, A. Andreanov, and S. Flach, Artificial flat band systems: From lattice models to experiments, *Adv. Phys.: X* **3**, 1473052 (2018).
- [41] L. Balents, C. R. Dean, D. K. Efetov, and A. F. Young, Superconductivity and strong correlations in Moiré flat bands, *Nat. Phys.* **16**, 725 (2020).
- [42] Y. Cao, V. Fatemi, S. Fang, K. Watanabe, T. Taniguchi, E. Kaxiras, and P. Jarillo-Herrero, Unconventional superconductivity in magic-angle graphene superlattices, *Nature (London)* **556**, 43 (2018).
- [43] T. Mizoguchi and M. Udagawa, Flat-band engineering in tight-binding models: Beyond the nearest-neighbor hopping, *Phys. Rev. B* **99**, 235118 (2019).
- [44] M. Qin, T. Schäfer, S. Andergassen, P. Corboz, and E. Gull, The Hubbard model: A computational perspective, *Annu. Rev. Condens. Matter Phys.* **13**, 275 (2022).
- [45] M. Iskin, Two-body problem in a multiband lattice and the role of quantum geometry, *Phys. Rev. A* **103**, 053311 (2021).
- [46] M. Iskin, Effective-mass tensor of the two-body bound states and the quantum-metric tensor of the underlying Bloch states in multiband lattices, *Phys. Rev. A* **105**, 023312 (2022).
- [47] L. Pricoupenko, Isotropic contact forces in arbitrary representation: Heterogeneous few-body problems and low dimensions, *Phys. Rev. A* **83**, 062711 (2011).
- [48] It is such that the binding energy  $E_2^{\text{be}}(\mathbf{q})$  of the dimer is always defined from an unbound pair of a free spin- $\downarrow$  fermion plus a free spin- $\uparrow$  fermion; the binding energy  $E_3^{\text{be}}(\mathbf{q})$  of the trimer is defined from the dimer threshold plus a free spin- $\uparrow$  fermion when  $E_2^{\text{be}}(\mathbf{q}) > 0$ ; the binding energy  $E_4^{\text{be}}(\mathbf{q})$  of the tetramer is defined from the trimer threshold plus a free spin- $\uparrow$  fermion when  $E_3^{\text{be}}(\mathbf{q}) > 0$ , etc.
- [49] P. Törmä, L. Liang, and S. Peotta, Quantum metric and effective mass of a two-body bound state in a flat band, *Phys. Rev. B* **98**, 220511(R) (2018).
- [50] S. D. Huber and E. Altman, Bose condensation in flat bands, *Phys. Rev. B* **82**, 184502 (2010).
- [51] L. G. Phillips, G. De Chiara, P. Öhberg, and M. Valiente, Low-energy behavior of strongly interacting bosons on a flat-band lattice above the critical filling factor, *Phys. Rev. B* **91**, 054103 (2015).
- [52] V. A. J. Pyykkönen, S. Peotta, P. Fabritius, J. Mohan, T. Esslinger, and P. Törmä, Flat-band transport and Josephson effect through a finite-size sawtooth lattice, *Phys. Rev. B* **103**, 144519 (2021).
- [53] S. M. Chan, B. Grémaud, and G. G. Batrouni, Pairing and superconductivity in quasi-one-dimensional flat-band systems: Creutz and sawtooth lattices, *Phys. Rev. B* **105**, 024502 (2022).
- [54] S. R. White, Density Matrix Formulation for Quantum Renormalization Groups, *Phys. Rev. Lett.* **69**, 2863 (1992).
- [55] U. Schollwöck, The density-matrix renormalization group in the age of matrix product states, *Ann. Phys.* **326**, 96 (2011).
- [56] M. Fishman, S. R. White, and E. M. Stoudenmire, The ITensor software library for tensor network calculations, [arXiv:2007.14822](https://arxiv.org/abs/2007.14822).
- [57] P. Weinberg and M. Bukov, QuSpin: A Python Package for Dynamics and Exact Diagonalisation of Quantum Many Body Systems. Part II: Bosons, Fermions and Higher Spins, *SciPost Phys.* **7**, 020 (2019).
- [58] M. Valiente, D. Petrosyan, and A. Saenz, Three-body bound states in a lattice, *Phys. Rev. A* **81**, 011601(R) (2010).
- [59] M. Iskin and A. Keleş, Dimers, trimers, tetramers, and other multimers in a multiband bose-hubbard model, [arXiv:2208.01429](https://arxiv.org/abs/2208.01429).